SPECTROSCOPIC PROPERTIES OF COOL STARS IN THE SDSS: AN ANALYSIS OF MAGNETIC ACTIVITY AND A SEARCH FOR SUBDWARFS

ANDREW A. WEST[1,2], SUZANNE L. HAWLEY[2], LUCIANNE M. WALKOWICZ[2], KEVIN R. COVEY[2], NICOLE M. SILVESTRI[2], SEAN N. RAYMOND[2], HUGH C. HARRIS[3], JEFFREY A. MUNN[3], PEREGRINE M. MCGEHEE[4,5], ŽELJKO IVEZIĆ[6,7], J. BRINKMANN[8]

ABSTRACT

We present a spectroscopic analysis of nearly 8000 late-type dwarfs in the Sloan Digital Sky Survey. Using the Hα emission line as an activity indicator, we investigate the fraction of active stars as a function of spectral type and find a peak near type M8, confirming previous results. In contrast to past findings, we find that not all M7-M8 stars are active. We show that this may be a selection effect of the distance distributions of previous samples, as the active stars appear to be concentrated near the Galactic Plane. We also examine the activity strength (ratio of the luminosity emitted in Hα to the bolometric luminosity) for each star, and find that the mean activity strength is constant over the range M0-M5 and declines at later types. The decline begins at a slightly earlier spectral type than previously found. We explore the effect that activity has on the broadband photometric colors and find no significant differences between active and inactive stars. We also carry out a search for subdwarfs using spectroscopic metallicity indicators, and find 60 subdwarf candidates. Several of these candidates are near the extreme subdwarf boundary. The spectroscopic subdwarf candidates are redder by ~ 0.2 magnitudes in $g-r$ compared to disk dwarfs at the same $r-i$ color.

Subject headings: solar neighborhood — stars: low-mass, brown dwarfs — stars: activity — stars: late-type — subdwarfs — Galaxy: structure

1. INTRODUCTION

Low mass stars with late spectral types (M,L) are the majority constituent of the Galaxy by number. Their main-sequence lifetimes are much greater than the current age of the Universe and they therefore serve as useful probes of Galactic star formation history in the local solar neighborhood (Gizis, Reid & Hawley 2002). They also encompass many important regions of stellar parameter space, including the onset of complete convection in the stellar interior, the onset of significant electron degeneracy in the core, and the formation of dust and subsequent depletion of metals onto dust grains in the stellar atmosphere. Of particular interest is the fact that many late-type stars have strong surface magnetic fields (Johns-Krull & Valenti 1996) that heat the outer atmosphere above the photosphere, and lead to observable emission from the chromosphere (e.g. Ca II and H Balmer series lines), the transition region (e.g resonance lines of abundant ions such as C IV), and the corona (e.g. thermal soft X-rays). The physics that controls the production of magnetic fields in low mass stars is not well understood, as the lack of a radiative-convective boundary layer precludes storing large scale fields as in a solar-type dynamo. However, recent work on turbulent dynamo mechanisms (Bercik et al. 2004) may soon provide new insight into the formation and properties of magnetic fields in low mass stars. The present study seeks to place strong empirical constraints on the magnetic activity in these stars, by measuring optical Hα emission in a sample of nearly

8000 low mass dwarfs. Our results will aid in the interpretation of the models and provide a connection to the physical processes occurring in the atmospheres of the stars.

The Hα emission line is produced by collisional excitation in the relatively dense chromospheres of these low mass, high gravity stars. Located in the red region of the optical spectrum, it is the strongest and best-studied indicator of magnetic activity in late type stars (in contrast to solar type stars which are usually studied in the Ca II H and K resonance lines). Previous results indicate that the fraction of M dwarfs with Hα emission increases from early to mid M spectral types (Joy & Abt 1974; Hawley, Gizis & Reid 1996), reaches a peak near type M7 where essentially all stars are active, and declines toward later types (Gizis et al. 2000a). The increasing fraction in the early to mid M types may be an age effect such that the activity lasts longer in the mid M types (Hawley, Reid & Tourtellot 2000a; Gizis et al. 2002), while the decline toward late M types may reflect difficulty in producing and/or maintaining surface magnetic fields due to the physics of turbulent dynamos and/or the increasingly neutral atmosphere (Hawley, Reid & Gizis 2000b; Fleming, Giampapa & Schmitt 2000; Mohanty et al. 2002). It does not appear that the atmosphere changes character such that Hα is no longer produced when magnetic activity is present in the later type stars. Indeed the ratio of Hα to transition region (C IV) and soft X-ray emission appears to be similar throughout the M dwarf spectral sequence (Hawley & Johns-Krull 2003).

Previous work also shows that the activity strength, measured

---

[1] Corresponding author: west@astro.washington.edu

[2] Department of Astronomy, University of Washington, Box 351580, Seattle, WA 98195

[3] US Naval Observatory, Flagstaff Station, P.O. Box 1149, Flagstaff, AZ 86002

[4] NMSU, Department of Astronomy, 1320 Frenger Mall, Las Cruces, NM 88003

[5] Los Alamos National Laboratory, MS H820, Los Alamos, NM 87545

[6] Princeton University, Princeton, NJ 08544

[7] H.N. Russell Fellow, on leave from the University of Washington

[8] Apache Point Observatory, P.O. Box 59, Sunspot, NM 88349

1

by the ratio of the luminosity in Hα to the bolometric luminosity (L_{H_α}/L_{bol}), is nearly constant (with large scatter) through the M0-M6 range (Hawley et al. 1996) and declines at later types (Burgasser et al. 2002, Cruz & Reid 2002). However, the sample of stars on which these conclusions are based numbers less than 100 for types M7 and later, due to the difficulty of obtaining spectra for these faint objects. Our sample in this crucial spectral type range is an order of magnitude larger, comprising more than 1000 stars with types between M7 and L0, and nearly 8000 stars between M0 and L0. This uniformly acquired and reduced sample from the Sloan Digital Sky Survey (SDSS), with well-characterized uncertainties, now allows us to obtain statistically significant magnetic activity results for the entire M dwarf spectral type range. In addition, we compare the photometric colors of the active and inactive stars to investigate whether the active stars are typically bluer at the same spectral type, an effect attributed to an increase in plage areas on active stars by Amado & Byrne (1997). Alternatively, such a correlation might indicate that micro-flaring activity plays a significant role in heating the outer atmospheres of active M dwarfs (cf. Güdel et al. 2003).

Our SDSS spectral sample is also well-suited for investigation of the incidence of low mass subdwarfs in the local neighborhood. Gizis (1997) showed that M subdwarfs could be identified by comparing the metallicity and gravity sensitive molecular bands of CaH and TiO. Using his technique, we identify dozens of new M subdwarf and extreme subdwarf candidates, and examine their colors in the SDSS *ugriz* filters.

2. DATA

The SDSS (York et al. 2000; Gunn et al. 1998; Fukugita et al. 1996; Hogg et al. 2001; Smith et al. 2002; Stoughton et al. 2002; Pier et al. 2003, Abazajian et al. 2003) is an excellent tool for spectroscopic studies of stars. Each spectroscopic plate produces 640 spectra with resolution $\lambda/\Delta\lambda = 1800$. Because all spectra are obtained and reduced through uniform pipelines with well understood uncertainties (York et al. 2000), it is possible to undertake statistically robust studies of very large samples. Our sample was selected from the SDSS spectroscopic and photometric databases as follows. In July 2002, the spectroscopic database was queried for all objects which satisfied the SDSS color cuts for late-type stars given in Hawley et al. (2002; hereafter H02), viz. $0.8 < (r-i) < 3.0$ and $0.3 < (i-z) < 3.5$. The photometry for the color cuts came from the preliminary SDSS photometric database[9] available at that time. This color cut yielded ∼ 17000 late-type star candidates with SDSS spectra. In April 2003 we added an additional ∼ 5000 candidates from spectroscopic observations that were specifically targeted for late type stars in the Southern Survey region. The final ∼ 22000 candidates come from 427 SDSS spectroscopic plates; 380 of the plates are in the SDSS Data Release 2 (DR2; Abazajian et al. 2004) sky area while 47 plates have yet to be publicly released. Due to recent improvements in the photometric reductions, we have used photometry only from the 5_4_25 version of Photo (SDSS photometric reduction software) in our final analysis. This is the same version used in the DR2 release.

3. ANALYSIS

3.1. *Spectral Types*

In order to assign spectral types to the stars in the sample, we pass each spectrum through two independent spectral typing pipelines. The first method determines the best fit, in a least squares sense, to both the SDSS late-type template spectra defined in H02 and the template spectra from the Keck and Apache Point Observatories used by H02 in their analysis; it is a derivative of the procedure originally described in Kirkpatrick (1991) and subsequently modified by Henry et al. (2002). The second method measures several molecular band indices in each spectrum and uses a weighted mean of the individual types from each index to assign a best-guess spectral type (cf. Reid, Hawley, & Gizis 1995a; Kirkpatrick et al. 1999). Both methods are described in detail in H02. Using the spectral typing pipeline outputs as a guide, each spectrum is individually inspected by eye and the assigned spectral type is altered as needed. As reported in H02, the uncertainty in this procedure is ∼ 1 spectral type. Spectra with a signal-to-noise ratio (SNR) < 5 are not typed, as experience shows that they do not give useful results in our analysis. Of the 22000 original candidates, ∼ 9200 were assigned M or L spectral types and had spectra with the necessary signal-to-noise ratio for further analysis. An important byproduct of the spectral typing procedure was the identification of numerous white dwarf - M dwarf binary systems in our sample. We find the binaries based on the appearance of blue continuum flux and features such as broad hydrogen Balmer absorption lines (Raymond et al. 2003). We have removed all such binaries from the final sample so that their colors will not affect our investigation of the colors of active vs. inactive M dwarfs, and because the nature of the M dwarf activity may be influenced by the presence of a close binary companion. §3.3 outlines a photometric test used to further constrain our sample to stars without white dwarf companions. Our sample is thus, as far as possible, composed of only single M dwarfs (or M dwarfs in binary systems with fainter M or L dwarfs that we are unable to discern from the spectra).

3.2. *Activity*

3.2.1. Hα *Measurements*

The SDSS spectra are spectrophotometrically calibrated, so we measure the Hα flux directly from each spectrum. The challenge is to automatically, but accurately, measure the flux in Hα over a range of spectral types with changing continuum slope and molecular features. Our procedure uses trapezoidal integration to sum the flux under the emission line, taking care to avoid and/or account for regions that are affected by local TiO features including the continuum bump just to the blue of Hα (Pettersen & Coleman 1981) and the absorption trough to the red (Tinney & Reid 1998; White & Basri 2003). We define a 14Å interval (7Å on either side of the line center) for the Hα flux calculation. We investigated several options to find the optimum continuum flux measure: a) the average over two 50Å sections (6500-6550Å and 6575-6625Å) on either side of the line; b) the average over two 10Å sections (6545-6555Å and 6575-6585Å) on either side of the line; and c) the blue 10Å region only, as used by Reid et al.(1995a) for the PMSU survey (6545-6555Å). We found no significant differences in the mean continuum values for these three measures, and therefore chose to use measure (a) as it is the most robust, and because we also use the 50Å regions as comparison for the equivalent width (EW) measurement (see below). The formal uncertainty

in the flux at each wavelength is available from the SDSS spectral calibration and is propagated at every stage of the analysis.

In order to be defined as active, each spectrum must pass the following criteria: 1) the Hα EW must be greater than 1.0Å; 2) the uncertainty in the EW must be smaller than the EW value; 3) the height of the Hα emission line must be 3 times the noise at line center; and 4) the EW of Hα must be 3 times larger than the average EW of the 50Å comparison regions. We examined subsets of the spectra that pass less conservative criteria, including those that passed only 2 or 3 of the 4 tests. These account for less than 5% of the total sample, and upon inspection are clearly marginal. There are 430 stars in the less conservative subsets that appear to be active but have Hα EW less than 1.0Å. We do not include these in our analysis but mention them as potential active stars similar to the stars in Groups C and E of Gizis et al. (2002). For the remainder of this paper all results reported will be from spectra that either passed all of the above criteria (active - 1910 stars) or failed all of our tests, including the tests with less stringent criteria (inactive - 5930 stars), for a total of 7840 stars in the final activity sample. Subdwarfs have also been removed from this sample; they are discussed separately in §4.4 below. We reiterate that in order to be classified as inactive, the Hα EW must be less than 1.0Å. Thus a star with Hα EW > 1.0Å, but with noisy data, is not classified as either active or inactive, but is simply removed from the sample. The H02 subset of 659 late type stars from the SDSS Early Data Release was analyzed with this method and then inspected by eye. We found that less than 4% of the stars were incorrectly labeled as active or inactive, and cite this as a measure of our ability to determine the activity status automatically.

3.2.2. *Quantifying Activity*

A star's magnetic activity can be qualitatively assessed as either active or inactive using the EW of the Hα emission line. However, because the EW measure depends on the flux in the local stellar continuum, it cannot be used to compare the strength of the activity in stars of different spectral type (Reid, Hawley, & Mateo 1995b). Instead, we measure activity strength by computing the ratio of the luminosity in Hα (L_{H_α}) to the bolometric luminosity (L_{bol}). The ratio L_{H_α}/L_{bol} is a measure of the magnetically driven radiative output compared to the total radiative output of the star, and does not depend on the shape of the stellar continuum.

In the past, L_{H_α} has been calculated by converting the measured Hα flux to a luminosity using the distance to the star. However, distance determinations for the stars in our sample rest on either spectroscopic or photometric parallax methods. To avoid introducing additional uncertainty into our L_{H_α} calculation due to uncertainties in the distances, we use a distance-independent method of calculating L_{H_α}/L_{bol}. The method is described in detail in Walkowicz et al. (2004) and uses well-observed nearby M and L dwarfs with known distances to empirically determine the ratio of the luminosity in the continuum at Hα, $L(\text{cont})_{H_\alpha}$, to the bolometric luminosity. The resulting ratios $\chi = L(\text{cont})_{H_\alpha}/L_{bol}$ are tabulated as a function of spectral type and color, and when multiplied by the EW in Hα for a given star, give the desired ratio L_{H_α}/L_{bol}.

Since the χ ratios are tabulated at 0.5 spectral type intervals, and we use integer spectral types in our analysis, a weighted mean of the χ values surrounding a given integer spectral type was computed. We give the two surrounding values 1/4 the weight of the integer χ value. This weight is also used in prop-

agating the uncertainties. We multiply each measured Hα EW by the appropriate mean χ factor and thereby calculate L_{H_α}/L_{bol} for each active star in our sample. Note that because there are no M0 stars in the nearby star sample, the M0 L_{H_α}/L_{bol} values in the present work have been calculated using only the M0.5 χ value.

3.3. *Colors*

The colors used in our analysis are formed from the *ugriz* psf magnitudes in the SDSS photometric database. As described above, we use photometry only from the latest (Fall 2003, Photo v. 5_4_25) pipeline reductions. To assure reasonable photometric accuracy, we include only stars with *u* magnitude uncertainties less than 0.3 and *griz* magnitude uncertainties less than 0.2 in our analysis of color effects. This decreases the number of stars available for analysis to ∼2200. However, if the *u* band data are not required, for example when examining $(g-r)$ colors, the sample numbers ∼5800. The maximum uncertainties in the colors that we use are therefore 0.36 magnitudes in $(u-g)$ and 0.28 magnitudes in $(g-r)$, $(r-i)$, and $(i-z)$. The great majority of stars in this color sample have uncertainties much smaller than these maximum values, with typical values being $\sigma(r) < 0.02$ for $r < 17$ (Ivezić et al. 2003; 11% of the sample); $\sigma(r) < 0.03$ for $r < 19$ (46% of the sample); and $\sigma(r) < 0.04$ for $r < 21$ (83% of the sample).

As discussed above, a significant source of scatter in the blue colors of the late type stars in our sample was introduced by the presence of numerous white dwarf - M dwarf binary systems. The spectroscopically-identified pairs were originally removed during the spectral typing process. In addition, we made a color cut on our sample, and included only stars whose colors lie outside the locus of known white dwarf - M dwarf pairs in the $(g-r)$ vs. $(u-g)$ color-color diagram (Silvestri, Hawley & Szkody 2003; Smolčić et al. 2004). In practice this meant that only stars with $(u-g) > 1.8$ are included in the sample. All suspected pairs based on either photometry or spectroscopy were therefore removed, and are not included in the final spectroscopic sample of 7840 stars.

3.4. *Molecular Band Indices*

To investigate the presence of metal poor stars in our sample, we use the varying strengths of the TiO and CaH molecular bands in a low metallicity environment. We measure the TiO5, CaH1 and CaH2 molecular band indices following the procedure outlined by Reid et al.(1995a). Gizis (1997) uses the same indices to define divisions between dwarfs, subdwarfs and extreme subdwarfs. In our study, the following criteria are used to restrict the sample of subdwarfs to high probability candidates: a) the band indices must be larger than their uncertainties (typical uncertainties are 0.04 in TiO5; 0.03 in CaH1; and 0.02 in CaH2); b) the band heights must be larger than both the noise in the continuum near the bandhead and the noise in the bottom of the absorption feature; and c) the computed uncertainties in the band indices must not overlap the subdwarf or extreme subdwarf boundaries.

4. RESULTS

4.1. *Activity Fraction vs. Spectral Type*

We find that in our sample of 7840 stars that are either active or inactive, 1910 are classified as active (24.4%). Figure 1 shows the fraction of stars which are active as a function of spectral type. The active fraction peaks at spectral type M8,

where 73% of stars are active. The numbers above each spectral type bin represent the total number of stars (both active and inactive) in the bin. The peak at M8 is consistent with Gizis et al. (2000a), who found a peak in the relation at types M7 and M8 using similar activity criteria. However, all stars in their sample were active at these types, while our results show $\sim 64-73\%$ of our M7-8 stars are active. We have confirmed by eye that indeed many of the M7 and M8 stars in our sample do not have measurable activity. Figure 2 shows examples of active and inactive M7 and M8 stars. The continuum features near Hα are noticeable in the inactive stars (blue bump, red trough), but it is clear that no measurable emission at Hα is present.

Following a suggestion by Neill Reid (private communication), we considered whether the disparity in active fraction at type M7 could be a distance effect. The Gizis et al.(2000a) sample was drawn from 2MASS and represents mostly nearby stars, while the SDSS sample described here extends to much greater distances due to the fainter limiting magnitude. We therefore restricted ourselves to just the M7 stars in the sample, and computed the distance to each star via the $(i-z)$ photometric parallax relation from H02. Only stars with good photometry ($\sigma(i-z) < 0.28$) were included (see §3.3), which reduced the sample from 777 to 269. Note that we did not combine stars of different spectral type (color) in the sample, so the relative distances between the M7 stars should be quite accurate, as uncertainties in the absolute calibration of the photometric parallax relation at different colors do not affect the calculation. We then computed the vertical distance, perpendicular to the Galactic Plane, for each star. The results are shown in Figure 3 for 60 pc distance bins. Though the number of stars in each bin is relatively small, leading to significant Poisson errors, there does appear to be a trend of decreasing active fraction with vertical distance from the Plane in both the North (positive) and South (negative) directions. If activity is related to age, as discussed by Hawley et al. (2000a) and Gizis et al. (2002), then this effect would be a natural consequence of the increasing velocity dispersion in older disk stars: the older stars would be more likely to be found further from the Plane where they were born. Kirkpatrick et al. (1994) first discussed the possibility that younger stars were found when looking South (toward the Plane, from the Sun's position 30 parsecs North of the Plane) than North, out of the Plane. Small sample sizes and uncertain distances precluded a definitive test using data available at that time, but we may now be seeing evidence for this effect in our much larger sample. The uncertainties are still large however, and more data are needed to verify this result. We plan to carry out a rigorous comparison between the 2MASS and SDSS samples to further investigate the correlation of activity fraction with distance from the Plane.

4.2. *Activity Strength vs. Spectral Type*

Figure 4 illustrates the activity strength, $\log(L_{H\alpha}/L_{bol})$, as a function of spectral type. Each histogram represents the distribution of $\log(L_{H\alpha}/L_{bol})$ at a given spectral type. The number to the right of the histogram is the peak value of the distribution. We see that $\log(L_{H\alpha}/L_{bol})$ peaks near -3.7 for stars of type M0-M5, in agreement with Hawley et al. (1996), and systematically peaks at lower activity strength among stars with later type. The 1Å Hα EW measurement limit in our sample imposes a lower limit on the measurable activity strength. At each spectral type the last bin (smallest $\log(L_{H\alpha}/L_{bol})$) with stars in it corresponds to this measurement limit. Table 1 gives

the $\log(L_{H\alpha}/L_{bol})$) corresponding to an H$\alpha$ EW of 1Å for each spectral type. Thus, the broader distributions seen at later types may be partly due to a selection effect. However, the distributions among the later types are quite symmetric and definitely declining at $\log(L_{H\alpha}/L_{bol})$ values that are easily measurable. Therefore it appears that the activity strength covers a larger range, and is less sharply peaked, among the later type stars.

Figure 5 shows the mean of the $L_{H\alpha}/L_{bol}$ distribution as a function of spectral type. The errors in this plot are the errors in the $L_{H\alpha}/L_{bol}$ calculation added in quadrature with the 1σ distribution of each bin. The dotted line indicates the $L_{H\alpha}/L_{bol}$ for an Hα EW of 1Å (the required minimum EW from §3.2). Table 1 gives the mean values for each spectral type. The approximately constant value from M0-M5 is clearly shown, as is the decline starting at types M5-M6. This decline occurs at a slightly earlier type than in previous studies, where the decline appeared at types M7-M8 (Gizis et al. 2000a; Burgasser et al. 2002).

4.3. *Colors and Activity*

We used several SDSS color-color diagrams to investigate the photometric properties of active stars. Figure 6 shows that the colors of the active stars are very similar to the inactive stars. It has been claimed previously that active stars are marginally bluer than inactive ones in the Johnson U-B color, with δ (U-B) = 0.04 ± 0.09 for late-type main-sequence dwarfs (Amado & Byrne 1997). They speculate that the effect could be due to the appearance of bright plage regions on the active stars. Our results for the SDSS $(u-g)$ color show a similar, but not statistically significant effect: $\delta(u-g) = 0.05 \pm 0.25$. In the $(g-r)$ color the effect has the opposite sign: $\delta(g-r)$ = -0.11 ± 0.16. The scatter in the color distribution is much larger than the mean offsets, and we therefore cannot confirm the hypothesis that plage regions are more prevalent on the active stars. A two-dimensional Kolmogorov-Smirnov test confirms that there is no significant difference between the active and inactive stars in any of the color-color diagrams.

4.4. *Subdwarfs*

Figure 7 (left panel) plots the CaH1 index versus the TiO5 index. The solid line denotes the dwarf/subdwarf boundary defined by Gizis (1997). The CaH1-TiO5 relation is valid only for TiO5 > 0.49 and therefore we have not extended the boundary beyond that value. We find 60 stars (crosses) that fall below the subdwarf boundary (and have uncertainties that do not cross the boundary as described above). Figure 7 (right panel) shows a similar plot for the CaH2 index. Again the solid line indicates the dwarf/subdwarf boundary and the dashed line is the boundary between the subdwarf and extreme subdwarf populations. Several of the stars are close to the extreme subdwarf boundary and warrant further observation. The subdwarf and extreme subdwarf candidates from this study are listed in Table 2.

The colors of the subdwarf candidates are compared to the normal disk population in Figure 8. The subdwarfs are clearly delineated in the $(g-r)$ color, with the median $(g-r)$=1.61, nearly 0.2 magnitudes redder than the normal disk dwarfs. This effect may be due to excess absorption in numerous hydride bands in the g bandpass, and has been seen previously in the Johnson (B-V) color (Hartwick 1977; Bergbusch & Vandenberg 1992; Gizis 1997; Dahn et al. 1995). Figure 9 shows the strong correlation between $(g-r)$ color and CaH1 band strength for stars with $r < 19.5$. The subdwarf candidates are clearly separated from the normal disk dwarfs in this diagram. This

allows subdwarf candidates to be chosen photometrically, for example in the SDSS spectral targeting pipeline, with reasonable success. Note that not all of the stars found here come from subdwarf targeting; some were serendipitous observations of objects targeted for other purposes.

5. SUMMARY

Using a sample of more than 22000 candidates from the SDSS spectroscopic database, 7840 late type stars were identified and used to investigate the magnetic activity in M and early L dwarfs. This sample is much larger than all previous samples used for this purpose. Our results show that:

1. The fraction of active stars rises monotonically from spectral type M0 to M8 and then declines monotonically to the latest types we measured (L3-L4).

2. Only $\sim 70\%$ of the M7 stars in our sample are active, which differs from previous studies showing 100% activity at spectral type M7. We suggest that the answer to this discrepancy may lie in the distance distributions of the samples used. Our results indicate the possibility that stars near the Galactic Plane are more likely to be active, as expected if activity depends on age.

3. The activity strength, as measured by $L_{H\alpha}/L_{bol}$, is approximately constant from types M0-M5, and declines at later types. The width of the distribution is relatively narrow at early types but broadens considerably at type M6 and later.

4. The average $(u-g)$ color is slightly bluer for active stars compared to inactive ones, while the average $(g-r)$ color is slightly redder. However, these differences are not statistically significant.

5. 60 new subdwarf candidates are identified spectroscopically by comparing the strengths of the TiO and CaH molecular bands. Several of the candidates lie near the extreme subdwarf boundary and may be interesting targets for future observations.

6. The subdwarf candidates have similar colors to the disk dwarfs except in the $(g-r)$ color, where the median subdwarf $(g-r)$ is almost 0.2 magnitudes redder than disk dwarfs at the same $(r-i)$ color. This effect allows subdwarfs to be chosen photometrically from the SDSS database.

6. ACKNOWLEDGMENTS

REFERENCES

Abazajian, K., et al. 2003, AJ, 126, 2081

Abazajian, K., et al. 2004, in preparation

Amado, P.J. & Byrne, P.B. 1997, A&A, 319, 967

Bercik, D.J., Abbett, W.P., Fisher, G.H., & Fan, Y. 2003, AGU Fall Meeting Abstracts, 536

Bergbusch, P.A. & VandenBerg, D.A. 1992, ApJS, 81, 163

Burgasser, A.J., Liebert, J., Kirkpatrick, J.D. & Gizis, J.E. 2002, AJ, 123, 2744

Cruz, K.L. & Reid, I.N. 2002, AJ, 123, 2828

Dahn, C.C., Liebert, J., Harris, H.C., & Guetter, H.H. 1995,The Bottom of the Main Sequence - And Beyond ed. C.G. Tinney (Berlin: Springer-Verlag), 239

Fleming, T.A., Giampapa, M.S., & Schmitt, J.H.M.M. 2000, ApJ 533, 372

Fukugita, M., Ichikawa, T., Gunn, J.E., Doi, M., Shimasaku, K., and Schneider, D.P. 1996, AJ, 111, 1748

Gizis, J.E. 1997, AJ, 113, 806

Gizis, J.E., Monet, D.G., Reid, I.N., Kirkpatrick, J.D., & Burgasser, A.J. 2000b, MNRAS 311, 385

Gizis, J.E., Monet, D.G., Reid, I.N., Kirkpatrick, J.D., Liebert, J., & Williams, R.J. 2000a, AJ 120, 1085

Gizis, J.E., Reid, I.N. & Hawley. S.L. 2002, AJ 123, 3356

Güdel, M., Audard, M., Kashyap, V. L., Drake, J. J., & Guinan, E. F. 2003, ApJ 582, 423

Gunn, J.E., Carr, M.A., Rockosi, C.M., Sekiguchi, M., et al. 1998, AJ, 116, 3040

Hartwick, F.D.A. 1977, ApJ 214, 778

Hawley, S.L., Covey, K.R. et al. 2002, AJ, 123, 3409

Hawley, S.L., Gizis, J.E., & Reid, I.N. 1996, AJ, 112, 2799

Hawley, S.L. & Johns-Krull, C.M. 2003 ApJ 588, L109

Hawley, S.L., Reid, I.N., & Gizis, J.E. 2000b, ASP Conf. Ser. 212: From Giant Planets to Cool Stars, 252

Hawley, S.L., Reid, I.N., & Tourtellot, J.G. 2000a, Very Low-mass Stars and Brown Dwarfs, ed. R. Rebolo & M. R. (Zapatero-Osorio:Cambridge), 109

Henry, T. J., Walkowicz, L. M., Barto, T. C., & Golimowski, D. A. 2002, AJ 123, 2002

Hogg, D.W., Schlegel, D.J., Finkbeiner, D.P., and Gunn, J.E. 2001, AJ, 122, 2129

Ivezić, Ž., Lupton, R.H., Anderson, S., et al. 2003, Proceedings of the Work-shop *Variability with Wide Field Imagers*, Mem. Soc. Ast. It., 74, 978

Johns-Krull, C.M. & Valenti, J.A. 1996, ApJ 459, L95

Joy, A.H. & Abt, H.A. 1974, ApJS, 28, 1

Kirkpatrick, J.D., Henry, T.H., McCarthy, D.W. 1991 ApJS 77, 417

Kirkpatrick, J.D., McGraw, J.T., Hess, T.R., Liebert, J., & McCarthy, D.W. 1994, ApJS, 94, 749

Kirkpatrick, J.D., Reid, I.N., Liebert, J., Cutri, R.M., Nelson, B., Beichman, C.A., Dahn, C.C., Monet, D.G., Gizis, J.E., & Skrustskie, M.F. 1999, ApJ 519, 802

Kirkpatrick, J.D., Reid, I.N., Liebert, J., Gizis, J.E., Burgasser, A.J., Monet, D.G., Dahn, C.C., Nelson, B., & Williams, R.J. 2000, AJ, 120, 447

Leggett, S.K., Allard, F., Berriman, G., Dahn, C.C., & Hauschildt, P.H. 1996, ApJS, 104, 117

Leggett, S.K., Allard, F., Geballe, T.R., Hauschildt, P.H., & Schweitzer, A. 2001, 548, 908

Mohanty, S., Basri, G., Shu, F., Allard, F. & Chabrier, G. 2002, ApJ, 571, 469

Pettersen, B.R. & Coleman, L.A. 1981 ApJ 251, 571

Pier, J.R., Munn, J.A., Hindsley, R.B., Hennessy, G.S., Kent, S.M., Lupton, R.H., and Ivezic, Z. 2003, AJ, 125, 1559

Raymond, S.N., Szkody, P., Hawley, S.L., Anderson, S.F.,Brinkman, J, Covey, K.R., McGehee, P.M., Schneider, D.P., West, A.A., & York, D.G. 2003,AJ, 125, 2621

Reid, I.N. & Gizis, J.E. 1997, AJ, 113, 2246

Reid, I.N. & Hawley, S.L. 2000, New Light on Dark Stars: Red Dwarfs, Low-Mass Stars, and Brown Dwarfs (New York, Springer-Praxis)

Reid I.N., Hawley, S.L., & Gizis, J.E. 1995a, AJ, 110, 1838

Reid I.N., Hawley, S.L., & Mateo, M. 1995b, MNRAS, 272, 828

Reid, I.N., Kirkpatrick, J.D., Gizis, J.E., & Liebert, J. 1999, ApJ, 527, L105

Silvestri, N.M., Hawley, S.L. & Szkody, P. 2003, AAS, 203, 4201

Smith, J.A., Tucker, D.L., Kent, S.M., et al. 2002, AJ, 123, 2121

Smolčić, V. et al. 2004, submitted to ApJL

Stoughton, C., Lupton, R.H., Bernardi, M., et al. 2002, AJ, 123, 485 (Early Data Release)

Tinney, C.G. & Reid, I.N. 1998 MNRAS 301, 1031

Walkowicz, L.M., Hawley, S.L., & West, A.A. 2004, in preparation

White, R.J. & Basri, G. 2003, ApJ, 582, 1109

York, D.G., Adelman, J., Anderson, J.E., et al. 2000, AJ, 120, 1579
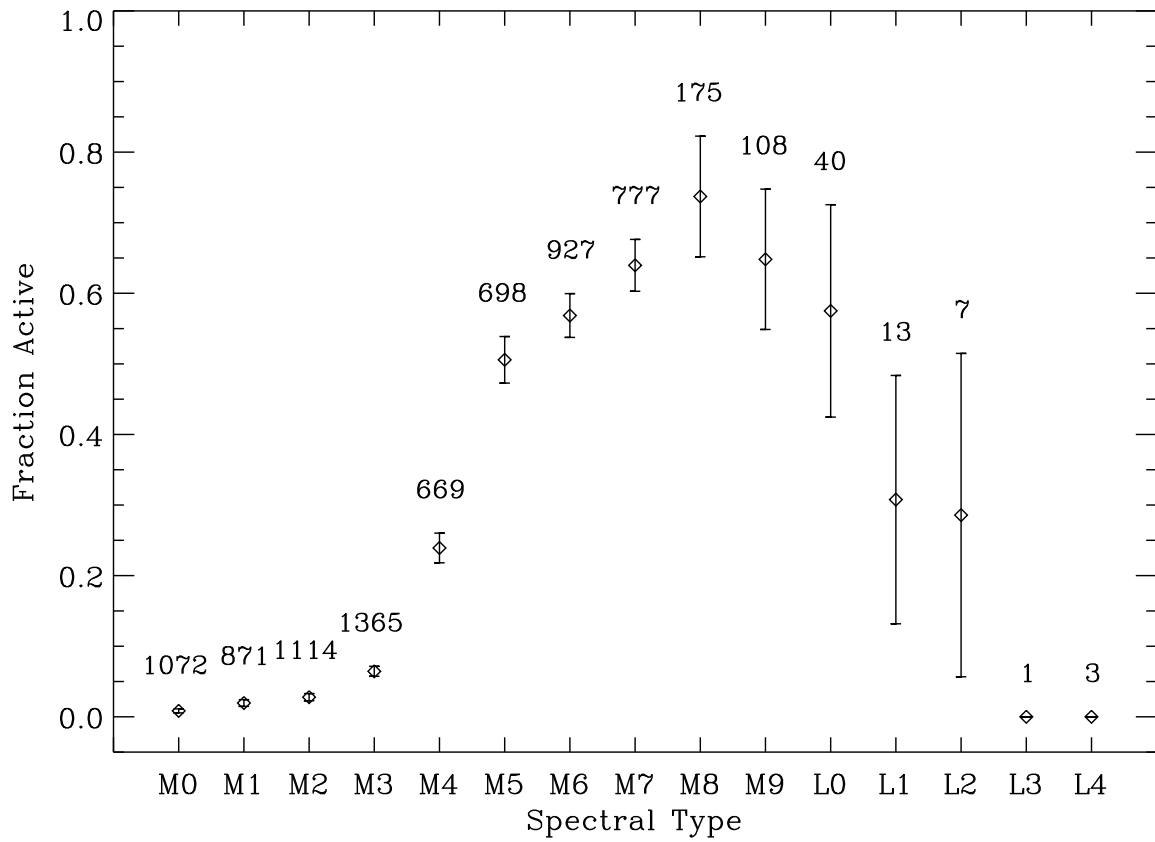
Fig. 1.— The fraction of active stars is shown as a function of spectral type. The numbers above each bin represent the total number of stars used to compute the fraction. The peak at spectral type M8 is consistent with previous results, but the presence of inactive M7 and M8 stars was not seen in earlier observations. Spectral type bins with no observed activity (L3, L4) are included for completeness.

8
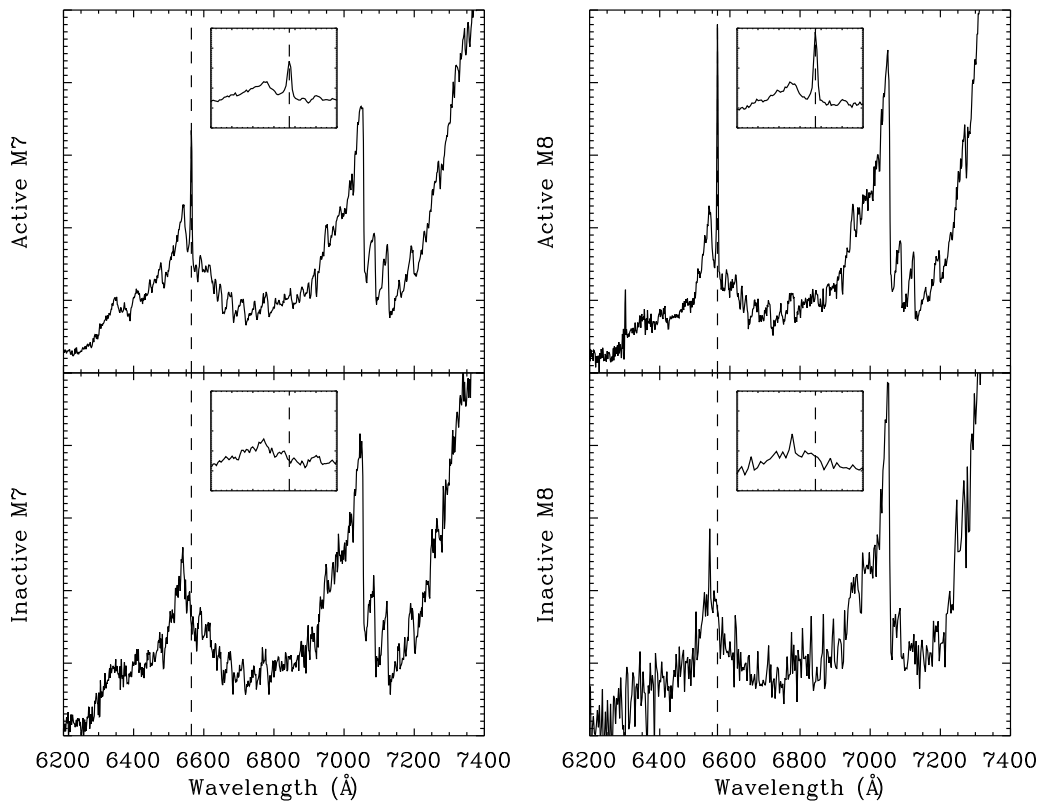
Fig. 2.— Active and inactive M7 (left panels) and M8 (right panels) stars. Small boxes in each panel contain a 100Å section of the spectrum near Hα. The dashed lines are drawn at the wavelength of Hα. Note that the line falls to the right of the closest spectral feature in both inactive spectra.
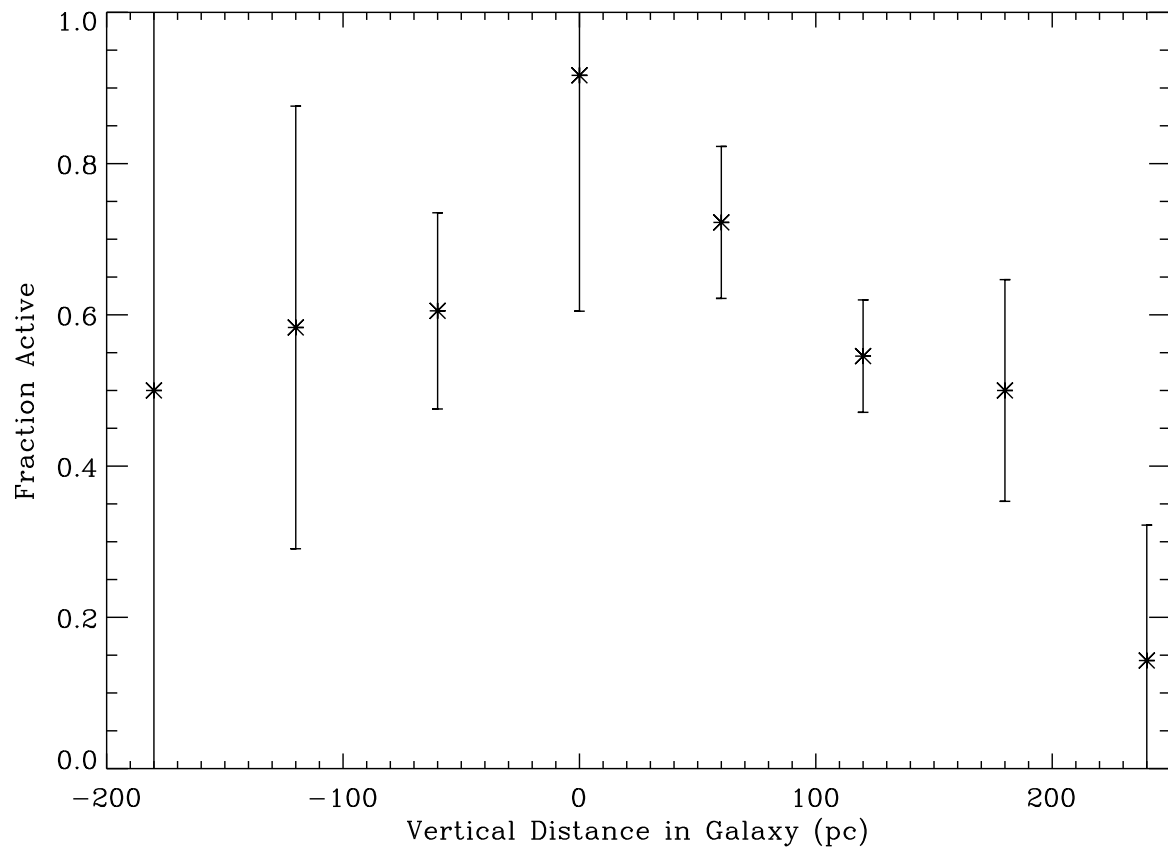
Fig. 3.— The fraction of M7 stars that are active is shown as a function of vertical distance above and below the Galactic Plane. Active stars appear to be concentrated toward the Plane, which may be an age effect (see text).
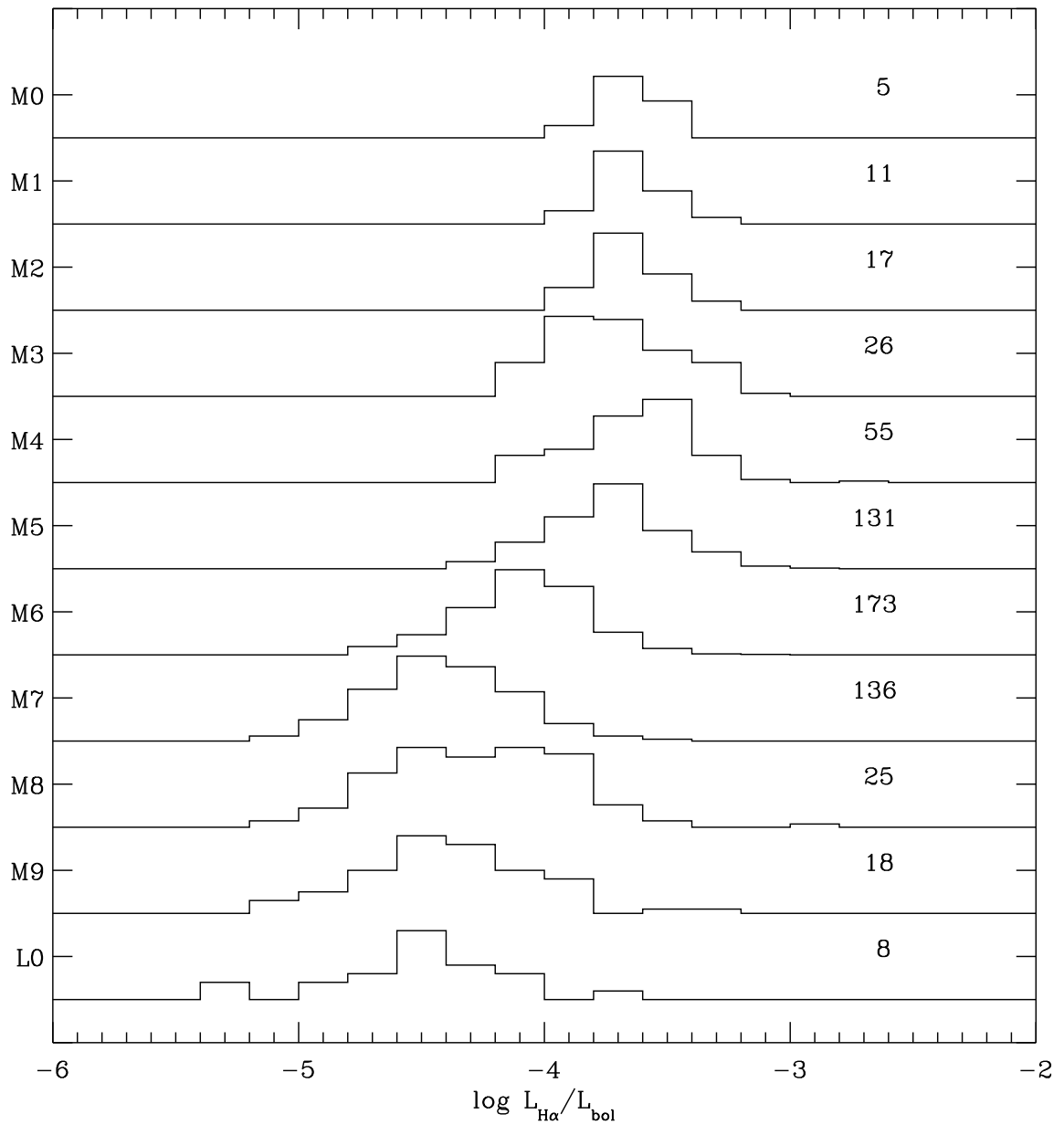
Fig. 4.— The distribution of the activity strength, $\log(L_{H\alpha}/L_{bol})$, is shown as a function of spectral type. The numbers to the right at each spectral type give the peak value of the histogram. The mean activity strength clearly declines at types M6 and later, and the distribution appears to broaden.
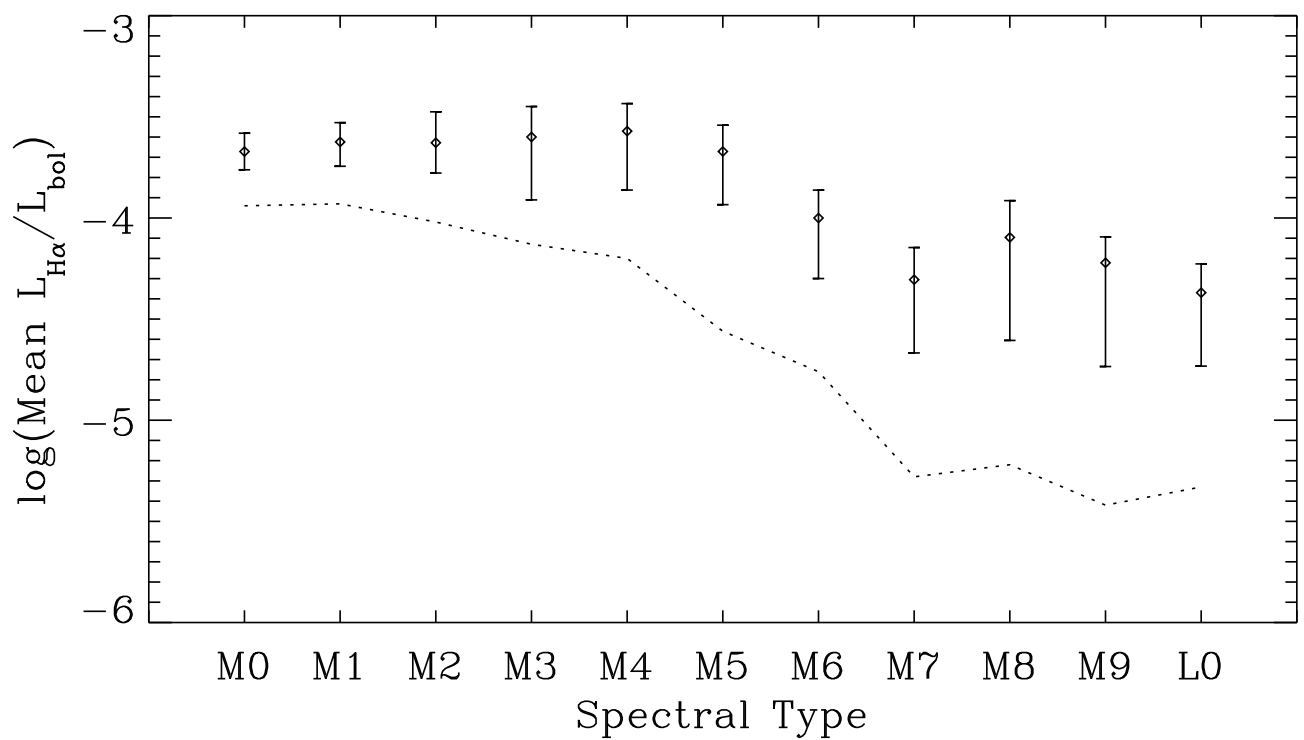
Fig. 5.— The mean activity strength, log(mean $L_{H\alpha}/L_{bol}$), is plotted as a function of spectral type. Uncertainties reflect the propagated errors in the calculation of $L_{H\alpha}/L_{bol}$ added in quadrature with the 1σ distribution of $L_{H\alpha}/L_{bol}$ in each bin. The decline in mean activity strength begins at spectral types M5-M6. The dotted line indicates the $L_{H\alpha}/L_{bol}$ value that we are sensitive to, due to the 1Å EW activity criterion.
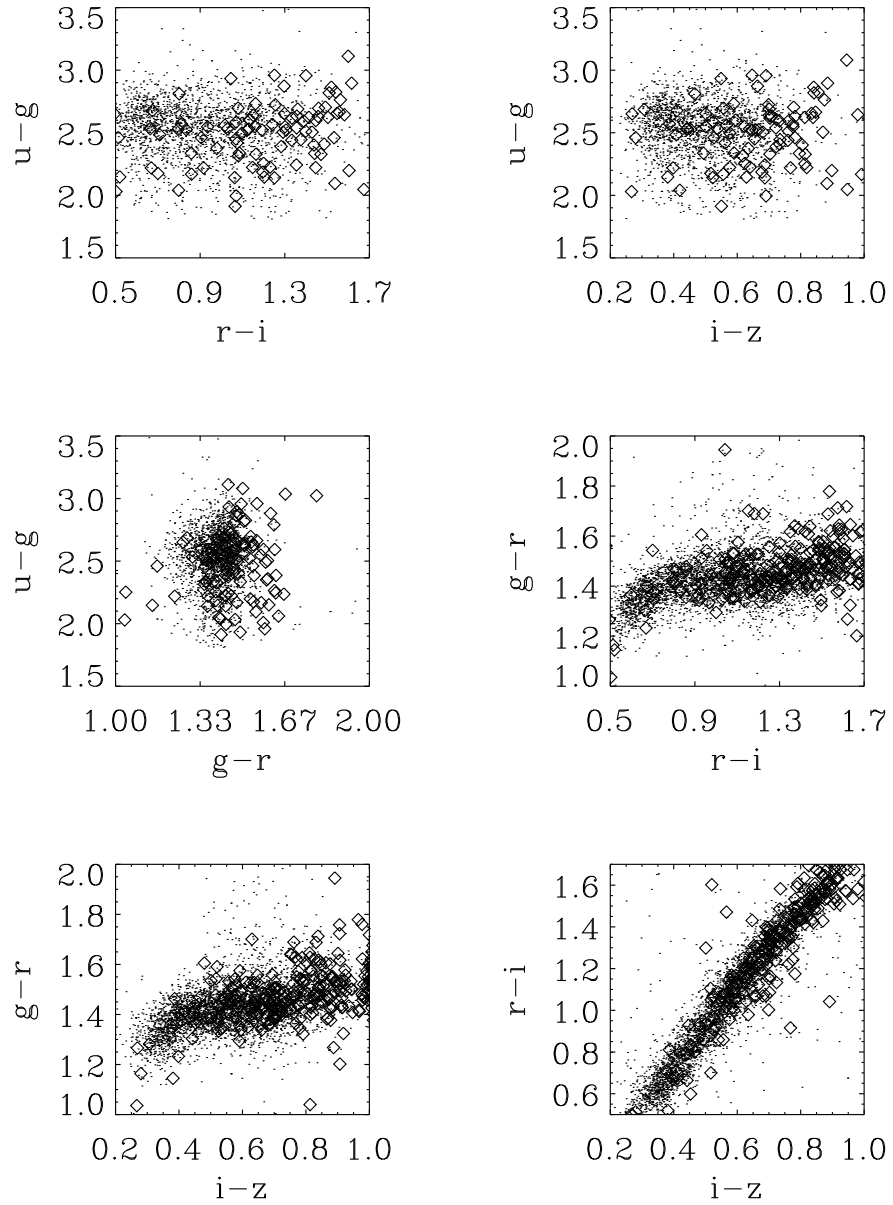
Fig. 6.— Several color-color diagrams in the SDSS *ugriz* filters are used to compare the colors of active stars (diamonds) to inactive stars (dots). A 2D KS test shows that there are no significant differences between active and inactive stars in any of the colors.
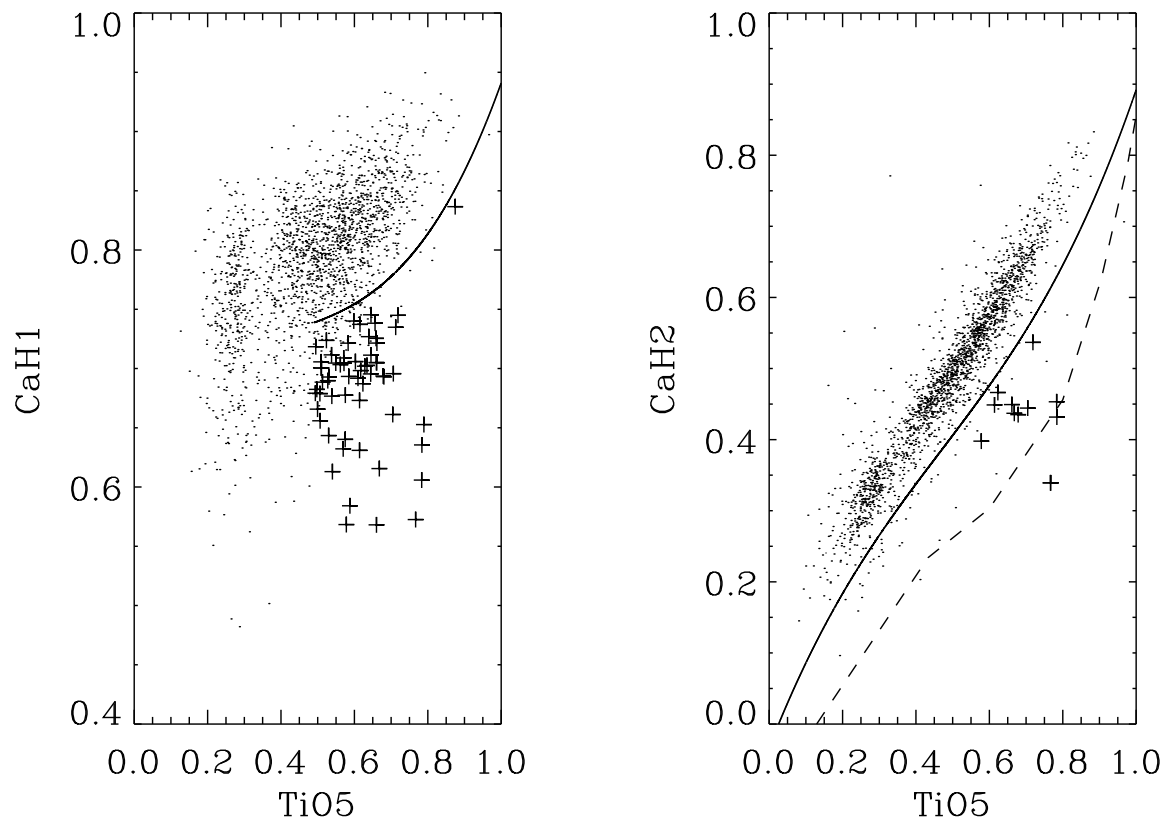
Fig. 7.— The left panel compares the CaH1 and TiO5 molecular band strengths, while the right panel compares CaH2 and TiO5. The solid line in each panel is the dwarf/subdwarf boundary from Gizis (1997). Crosses are subdwarf candidates that meet the criteria defined in §3.4.
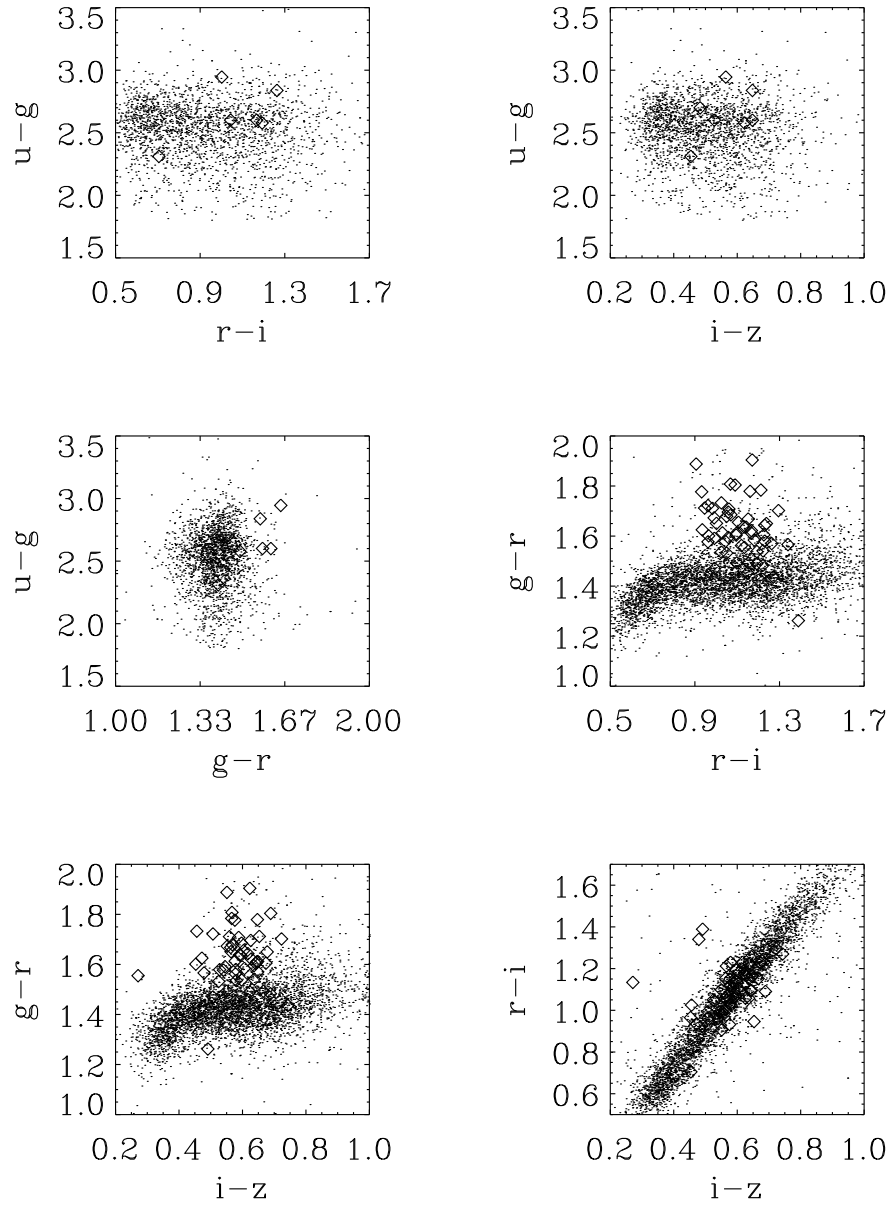
Fig. 8.— These SDSS color-color diagrams compare the colors of subdwarf candidates (diamonds) with normal disk dwarfs (dots). The $(g-r)$ colors of the subdwarf candidates are systematically redder at a given $(r-i)$ and $(i-z)$ color.
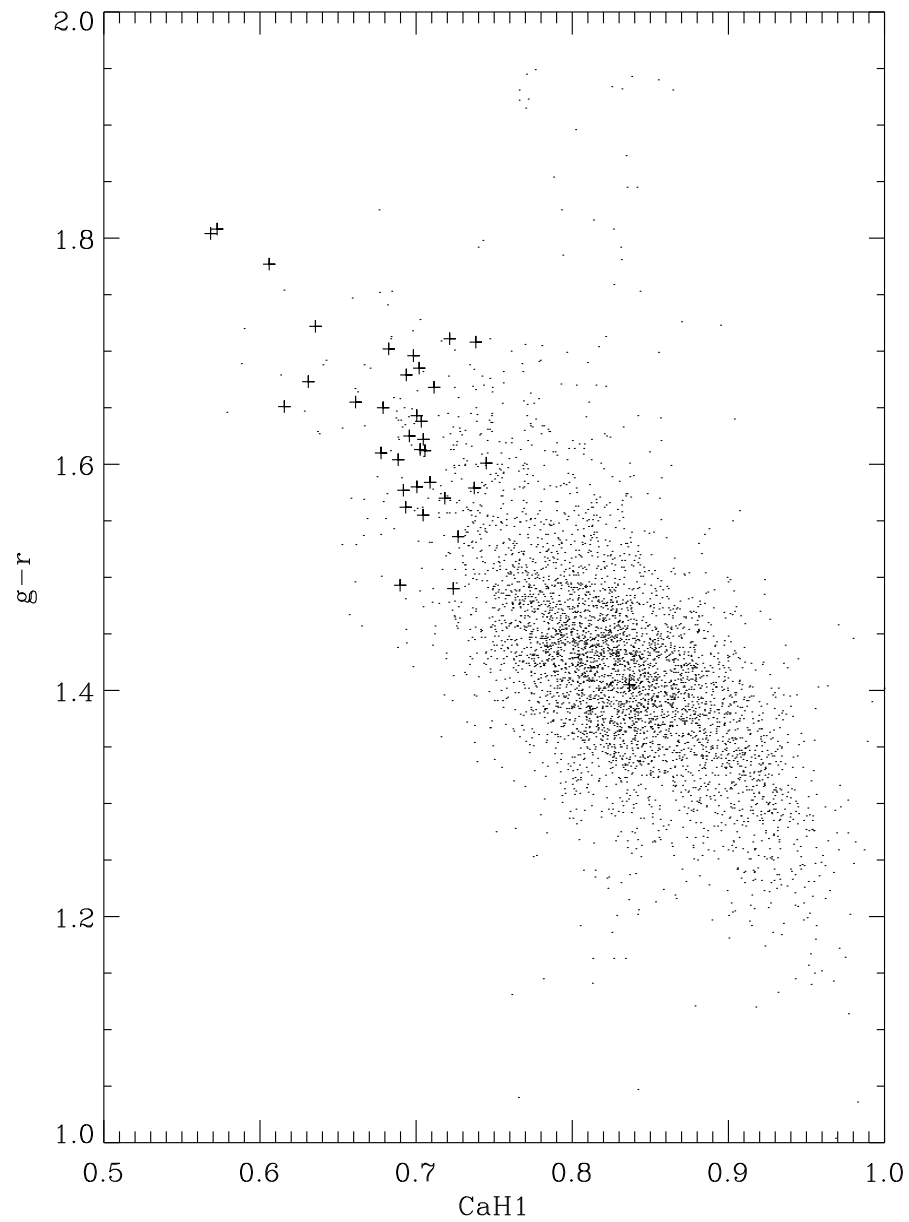
Fig. 9.— The redder $(g-r)$ colors of the subdwarf candidates are clearly evident in the $(g-r)$ vs. CaH1 diagram. The SDSS $(g-r)$ color provides a good photometric proxy for measuring strong hydride bands and allows subdwarfs to be identified photometrically. To reduce the photometric scatter, only stars with $r < 19.5$ are shown.

TABLE 1
$L_{H\alpha}/L_{bol}$ VS. SPECTRAL TYPE

Spectral Class	log(mean $L_{H\alpha}/L_{bol}$)	log($L_{H\alpha}/L_{bol}$) for 1Å EW
M0	-3.67	-3.94
M1	-3.62	-3.93
M2	-3.63	-4.02
M3	-3.60	-4.13
M4	-3.57	-4.20
M5	-3.67	-4.56
M6	-4.00	-4.76
M7	-4.31	-5.28
M8	-4.10	-5.22
M9	-4.22	-5.42
L0	-4.37	-5.33

TABLE 2
SUBDWARF DATA

Name	r^{ab}	$g-r^{ab}$	$r-i^{ab}$	$i-z^b$	TiO5	CaH1	CaH2	Hα EW (Å)[c]	Sp. Type
SDSS J002228.00−091444.8	18.92	-0.89	3.44	0.48	0.65	0.71	0.52	1.16	1
SDSS J003541.84+003210.1	20.15	1.64	1.14	0.59	0.68	0.69	0.54	-0.16	3
SDSS J003701.37−003248.3	20.15	1.60	1.23	0.67	0.57	0.64	0.46	-0.23	3
SDSS J003755.20−002134.2	18.70	—	1.01	0.89	0.65	0.75	0.57	-0.35	1
SDSS J010811.89+003042.4	17.34	1.61	1.17	0.65	0.51	0.71	0.45	-0.43	3
SDSS J012853.17+003356.6	19.34	1.56	1.12	0.58	0.58	0.69	0.50	-0.21	3
SDSS J014631.67+001658.3	19.79	1.26	1.39	0.49	0.58	0.72	0.48	-0.18	3
SDSS J020753.57−001958.8	20.16	1.54	1.22	0.64	0.50	0.67	0.46	0.02	3
SDSS J021956.49+005153.6	19.27	1.60	0.97	0.45	0.72	0.74	0.54	2.97	2
SDSS J022221.54+005430.3	19.01	1.64	1.13	0.59	0.56	0.70	0.46	0.04	3
SDSS J024501.77+003315.8	19.38	1.54	1.03	0.58	0.64	0.73	0.51	—	1
SDSS J031314.28−000619.8	20.33	1.48	1.22	0.69	0.51	0.66	0.51	-3.27	2
SDSS J032749.80−004445.4	19.88	1.59	0.99	0.55	0.64	0.70	0.62	-0.35	2
SDSS J033408.64−072349.2	20.21	1.89	0.91	0.55	0.79	0.65	0.45	-0.85	2
SDSS J081329.95+443945.6	19.39	1.68	1.07	0.60	0.63	0.70	0.50	-0.45	2
SDSS J082230.00+471645.8	19.39	1.67	1.15	0.56	0.54	0.71	0.46	0.04	2
SDSS J083002.73+483251.6	19.92	1.90	1.17	0.62	0.53	0.69	0.45	1.89	3
SDSS J083217.77+522408.2	19.61	1.49	1.10	0.55	0.60	0.71	0.52	-0.38	2
SDSS J084105.39+032109.6	20.05	1.45	1.15	0.58	0.62	0.69	0.47	0.24	3
SDSS J085843.89+511210.1	20.00	1.53	1.05	0.52	0.66	0.70	0.60	-0.98	2
SDSS J090238.75+471813.6	19.97	1.73	1.02	0.46	0.66	0.71	0.64	-0.58	2
SDSS J090434.02+513153.9	19.40	1.78	0.93	0.58	0.78	0.61	0.45	-0.64	1
SDSS J091451.98+453152.8	19.02	1.64	1.23	0.62	0.51	0.70	0.50	-0.58	3
SDSS J092429.76+523410.7	18.70	1.67	0.99	0.55	0.61	0.63	0.45	-0.47	2
SDSS J092534.16+524442.4	19.79	1.71	0.95	0.65	0.71	0.73	0.58	-0.61	3
SDSS J092708.10+561648.1	19.37	1.62	0.93	0.47	0.71	0.70	0.62	-0.41	1
SDSS J092745.78+582122.7	20.47	1.78	1.21	0.57	0.59	0.58	0.55	-0.86	3
SDSS J093024.66+554447.7	19.14	1.56	1.13	0.27	0.57	0.70	0.48	-0.21	3
SDSS J093141.85+453914.5	19.45	1.58	0.96	0.54	0.61	0.69	0.57	-0.41	2
SDSS J094306.37+465701.4	19.74	1.59	1.06	0.64	0.54	0.61	0.50	-1.34	3
SDSS J095147.77+003612.0	18.27	1.58	1.04	0.53	0.62	0.74	0.53	-0.35	2
SDSS J100109.54+015450.2	19.12	1.71	0.98	0.56	0.66	0.72	0.45	-0.62	2
SDSS J101031.13+651327.6	19.39	1.68	1.05	0.57	0.68	0.69	0.44	2.80	1
SDSS J104320.47+010439.4	19.16	1.66	1.11	0.60	0.70	0.66	0.44	—	2
SDSS J105122.43+603844.8	17.15	1.65	1.00	0.56	0.67	0.62	0.44	-0.17	2
SDSS J112751.35−001246.8	20.03	—	1.07	0.65	0.66	0.73	0.56	—	1
SDSS J113501.76+033720.3	—	—	—	—	0.53	0.64	0.53	—	3
SDSS J115900.70+665214.3	19.37	1.61	1.09	0.65	0.58	0.68	0.47	-0.53	3
SDSS J120724.85+004346.4	18.10	1.49	1.19	0.62	0.52	0.72	0.49	-0.44	3
SDSS J121510.41+003342.7	18.00	1.41	0.70	0.45	0.87	0.84	0.77	-0.19	0
SDSS J125919.29−025402.3	—	—	—	—	0.60	0.74	0.52	-0.39	2
SDSS J143930.77+033317.3	19.38	1.80	1.09	0.69	0.58	0.57	0.40	-0.85	3
SDSS J145447.32+011006.8	20.35	1.44	1.27	0.74	0.57	0.63	0.55	-0.57	3
SDSS J145547.00+602837.3	19.18	1.70	1.06	0.63	0.62	0.70	0.47	-0.28	2
SDSS J150511.33+620926.3	18.61	1.81	1.07	0.57	0.77	0.57	0.34	-0.38	3
SDSS J161348.84+482016.0	18.30	1.72	0.96	0.51	0.78	0.64	0.43	-0.34	1
SDSS J171745.22+625337.0	18.66	1.65	1.24	0.68	0.51	0.68	0.42	0.10	3
SDSS J173452.52+603603.1	18.78	1.71	1.06	0.59	0.66	0.74	0.55	-0.28	2
SDSS J215937.69+005536.2	18.96	1.61	1.03	0.58	0.63	0.70	0.53	—	2
SDSS J221500.88+005217.2	19.08	1.60	1.09	0.64	0.51	0.69	0.49	-0.28	2
SDSS J221625.03−003122.5	19.28	1.58	1.18	0.61	0.57	0.71	0.53	-0.49	3
SDSS J223802.82−082532.4	19.71	1.78	1.16	0.65	0.49	0.68	0.45	-0.65	3
SDSS J224605.41+141640.6	17.00	1.57	1.26	0.65	0.49	0.72	0.45	-0.41	3
SDSS J224854.83−091723.2	19.85	1.57	1.34	0.48	0.54	0.68	0.50	-0.21	3
SDSS J225538.34−005945.2	19.89	1.47	0.99	0.51	0.61	0.67	0.55	0.21	1
SDSS J230303.49−010656.7	18.95	1.62	1.17	0.63	0.55	0.70	0.50	-0.40	3
SDSS J230805.24+001812.7	19.36	1.70	1.30	0.72	0.50	0.68	0.42	-0.49	3
SDSS J233030.19+004521.9	19.45	1.58	1.23	0.58	0.51	0.70	0.46	-0.80	3
SDSS J235116.25−003104.8	19.48	1.49	1.15	0.67	0.53	0.69	0.45	-1.30	3
SDSS J235830.60−011413.2	19.99	1.54	1.19	0.60	0.66	0.57	0.49	-0.61	2

[a]Photometry is omitted when uncertainties are larger than 0.2 magnitudes.

[b]Photometry is not available for some objects.

[c]EWs of subdwarfs that were either classified as active or inactive (see Section 3.2) are included.